

# A New Transformer for High Voltage Charging Power Supply

Jianming Liu, Meng Wang, Fucai Liu

College of Electrical Engineering, Yanshan University, Qinhuangdao, China

Corresponding author, e-mail: ppkkkk@126.com

## Abstract

In this paper, the authors present a new high-frequency transformer for high-voltage capacitor charging power supply. They also establish a new topology structure and the charging control strategy for the charging power supply. The effects of leakage inductance and distributed capacitance by using the soft switching in the transformer were then analyzed. Finally, the different leakage inductances in the two transformers were tested. The results of the above study provide a theoretical basis for the application of the new high frequency transformer in pulsed power supply.

**Keywords:** charging power supply, distributed capacitance, transformer, leakage inductance

Copyright © 2014 Institute of Advanced Engineering and Science. All rights reserved.

## 1. Introduction

In recent years, the pulse forming network (PFN) of capacitor energy storage type is widely used in intense particle beam, X ray fields and electromagnetic launch [1]. The high-voltage capacitor charging power is an important part of PFN [2]. With the development of pulse conversion technology [3], the high-frequency charging technology has been rapidly applied [4]. The series resonant constant-current source plays an important role in the high-frequency charging technology. It gives the charging system higher efficiency, more precision and more miniaturization [5]. Now, the majority capacitor charging power supply is charged by the LC series resonance constant-current source. The capacitor power supply developed by the United States National Ignition Facility (NIF) is charged with a soft switching charging mode. Its maximum charge voltage is 24kV, charging rate is 25KW. The main circuit of the 70KW/24KV capacitor charging power supply developed by Germany is single inverter series resonant type [6]. The high frequency transformer of large power is the core component of capacitor constant-current charging power supply. How to select the distributed capacitance, the turns ratio of the transformer, magnetic flux density and winding process are important in the design of the high-frequency transformer [7-10].

## 2. The Simulation and Control Strategy

The main circuit structure of the capacitor charging power supply by using the series resonant is shown in Figure 1.

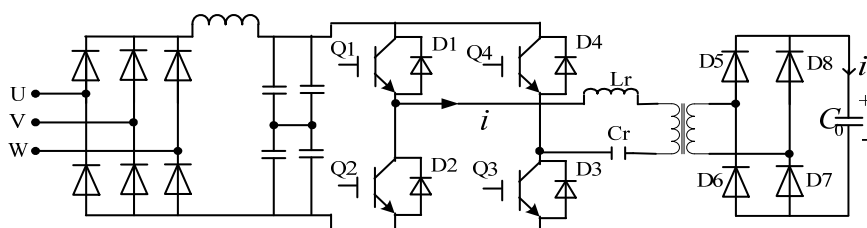


Figure 1. The circuit structure of CCPS

$n$  is the ratio.  $T_s$  is switching cycle. The resonance period  $T_r = 2\pi\sqrt{L_r * C_r}$ .  $f_s$  is switching frequency. The resonant frequency  $f_r = 1/(2\pi\sqrt{L_r * C_r})$ ,  $V_{in}$  is the rectified voltage. When  $f_s \leq f_r/2$ , the circuit is discontinuous. The conduction time of IGBT is within  $T_r \geq T \geq T_r/2$ . When  $n^2 C_0 \gg C_r$ , the charging current average value of the secondary side is:

$$I_0 = \frac{8V_{in}f_s C_r}{n} \quad (1)$$

When  $V_{in} = 500V$ ,  $f_s = 10KHz$  and  $f_r = 22KHz$ , the outputs of the current from the resonance and the rectifier are shown in Figure 2. The capacitor voltage and the envelope of the charging current are shown in Figure 3.

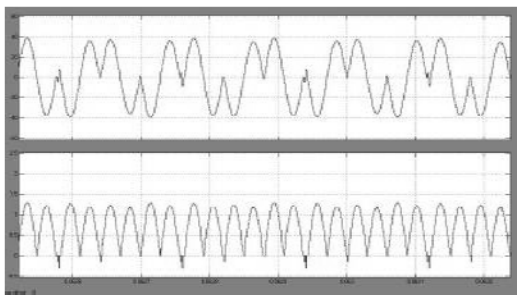


Figure 2. The Waveforms of the Current

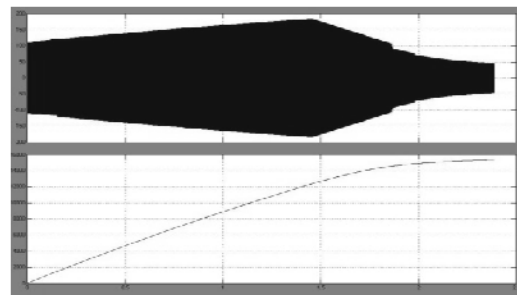


Figure 3. Resonant Current and Inverter Voltage

When  $f_r/2 < f_s < f_r$ , the resonant current and the charging current are continuously switched at the zero current point (ZCP). The two switch tubes in the same bridge arm are forced to be converted when the switch is turn-on. There are switching losses and noise here. When  $f_s > f_r$ , the main circuit is continuous. There are more switching losses and larger noise here. Due to the presence of inductance circuit, the switching device is often damaged by the higher peak voltage. The outputs of the current are shown in Figure 4.

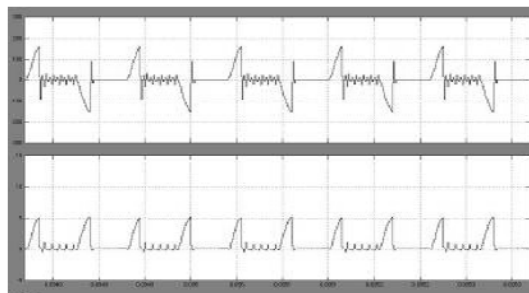


Figure 4. The Current with Width-modulated

### 3. The Influence of Distributing Parameters

#### 3.1. The Transformer Model

The permeability  $\mu$  of the transformer core actually is not infinite, the core reluctance  $R_m = L/\mu S$  is not zero. The equivalent circuit of transformer is shown in Figure 5.

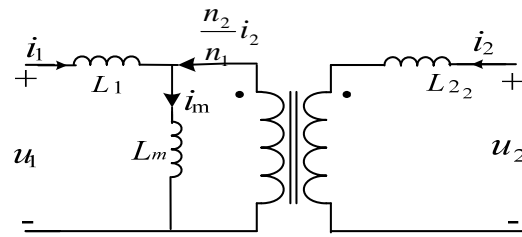


Figure 5. Equivalent Circuit of Transformer

$u_1$  and  $u_2$  are voltages.  $n_1$  and  $n_2$  are numbers of turns.  $i_1$ ,  $i_2$  and  $i_m$  are currents.

$$\phi R_m = n_1 i_1 + n_2 i_2, \quad (2)$$

$$u_1 = n_1 \frac{d\phi}{dt} \quad u_2 = n_2 \frac{d\phi}{dt} \quad (3)$$

$$u_1 = \frac{n_1}{R_m} \frac{d(n_1 i_1 + n_2 i_2)}{dt} = L_m \frac{di_m}{dt} = \frac{n_2}{R_m} \frac{d(n_1 i_1 + n_2 i_2)}{dt} = \frac{n_2}{n_1} L_m \frac{di_m}{dt} \quad (4)$$

$L_m = \frac{n_1^2}{R_m}$ .  $i_m = i_1 + \frac{n_2}{n_1} i_2$ .  $\phi_1$  is leaking magnetic flux of  $i_1$ .  $\phi_2$  is leaking magnetic flux of  $i_2$ .  $L_1 = n_1 \times d\phi_1 / di_1$ ,  $L_2 = n_2 \times d\phi_2 / di_2$ . The voltages of windings are:

$$u_1 = n_1 \frac{d(\phi + \phi_1)}{dt} = n_1 \frac{d\phi}{dt} + n_1 \frac{d\phi_1}{di_1} \frac{di_1}{dt} = n_1 \frac{d\phi}{dt} + L_1 \frac{di_1}{dt} \quad (5)$$

$$u_2 = n_2 \frac{d(\phi + \phi_2)}{dt} = n_2 \frac{d\phi}{dt} + n_2 \frac{d\phi_2}{di_2} \frac{di_2}{dt} = n_2 \frac{d\phi}{dt} + L_2 \frac{di_2}{dt} \quad (6)$$

By Equation (3) and (4),  $u_1$  and  $u_2$  are:

$$u_1 = L_m \frac{d}{dt} \left( i_1 + \frac{n_2}{n_1} i_2 \right) + L_1 \frac{di_1}{dt} \quad (7)$$

$$u_2 = \frac{n_2}{n_1} L_m \frac{d}{dt} \left( i_1 + \frac{n_2}{n_1} i_2 \right) + L_2 \frac{di_2}{dt} \quad (8)$$

The primary leaking inductance is:

$$\frac{1}{2} u_0 \int H^2 dv = \frac{1}{2} L_1 i_1^2 \quad (9)$$

$\mu_0$  is the permeability of vacuum.  $H$  is the intensity of the permeability in the leaking magnetic field.  $dv$  is the volume of the distributing element in the leaking magnetic field.

### 3.2. The Model of Distributed Capacitance

The distributed capacitances in the primary winding are  $C_1$ ,  $C_2$  and  $C_{12}$ . The model of the transformer with the distributed capacitance is shown in Figure 6.

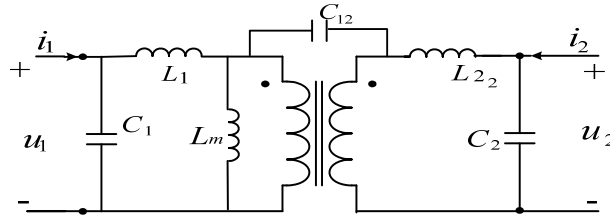


Figure 6. The Model of Transformer Including Leakage Inductance

## 4. The New High Frequency High Voltage Transformer

### 4.1. The Selection of Magnetic Core

The new transformer is made of microcrystalline, Fe-Ni amorphous, Po-Mo alloy, Mn-Zn ferrite and so on. Microcrystalline alloy has the advantages of lower price, higher saturation magnetization, lower coercivity and good thermal stability. Its parameters are shown in Table 1.

Table 1. Core Parameters

Saturation magnetic flux density	Residual magnetic flux density	Permeability
1.25T	<0.2T(20khz)	20000
Coercivity 1.60A/m	Working frequency 150khz	Curie temperature 570 <sup>0</sup> C

The maximum magnetic inductance strength  $B_m$  must be less than the saturation magnetic flux density  $B_s$ . It can prevent that power system to be briefly saturated when the power supply is turn-on. It can reduce the excitation current also. The magnetic flux density  $B$  of the Nanocrystalline alloy should meet the condition of  $2B \leq B_s - B_r$ . Usually  $B = B_m/3$ .  $B_r$  is the residual flux density.  $A_p$  is the product in the effective cross-sectional area  $A_e$  and the window core area  $A_w$ . The core size can be look-up from  $A_p$  in the Table 1.

$$A_p = \frac{1.16P_1}{4Bf_s K_0 K_j} = \frac{1.16 \times 10 \times 10^3 \times 2.1 \times 10^4}{4 \times 0.4 \times 10 \times 10^3 \times 0.4 \times 230} = 165(\text{cm}^2) \quad (10)$$

$P_1 = P_0(1/\eta + 1)$ .  $P_0$  is the output power. The work efficiency  $\eta = 0.9$ .  $B$  is the flux density.  $f_s$  is the working frequency. The pace factor of the window  $K_0$  is 0.4. The coefficient  $K_j$  approximately is 230. The ratio of primary and secondary is selected in 1:30.

### 4.2. The Effects of Winding Structure

The winding is wound in series form on the grooves of the skeleton in secondary side. The winding is wound by Z-shape. The structures of the two different winding in transformer  $T_1$  and  $T_2$  are designed. The diagram of the Z-type winding is shown in Figure 7(a). The top view of the core winding is shown in Figure 7(b). The secondary framework is made with 12 winding grooves. The secondary coil is divided into 10 sections around the 10 winding grooves (the

other two grooves are for the incoming and outgoing). There are 6 turns in each winding groove. The capacitance can be greatly decreased in the secondary layer by above design.

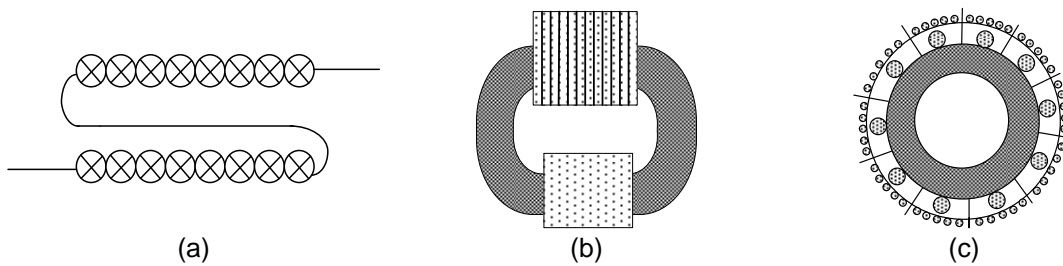


Figure 7. The Different Winding Dispositions of Transformer (a) The winding of the type Z ;(b) The winding of  $T_1$  ;(c) The winding of  $T_2$

The C-type super microcrystalline core is used to guarantee the insulation between the primary and the secondary. The primary and the secondary windings are completely isolated in the core and encapsulated by epoxy resin. The high-frequency transformer  $T_1$  is shown in Fig.8(a). In the actual high voltage charging experiment, the inter-turn of the secondary winding was breakdown two times. The breakdown positions were at the end of the winding. This is due to the existence of distributed capacitance and the unbalanced distribution of electric potential. In the improved transformer, these problems are solved by reducing the number of turns on monolayer and adding insulation material between the layers. To reduce the leakage inductance, the insulation level between the primary and secondary windings is increased. It will make the coupling coefficient reducing and the leakage inductance to be increase. The actual measured leakage inductance  $L_m=125\mu H$ . When the leakage inductance of the transformer is larger, the leakage inductance is directly involved in the resonance in the actual test. The resonant inductor is not involved in this condition. The range of the switch frequency  $f_s$  is limited by the higher leakage inductance. The resonant current is smaller. It can be explained by the soft switch control strategy [11]. The output of the actual power can only be 50%-60%. The leakage inductance can be reduced by using the tight coupling between the primary and the secondary winding. The parasitic capacitance can be reduced by the series winding on the secondary. The nanocrystalline toroidal iron core is selected for it. The top view of the winding is as shown in Figure 7(c). The primary and secondary windings uniformly are wound on the same core. The secondary winding are wound around the primary outer within the multi-groove framework. The primary and the secondary windings are isolated by epoxy resin. The wound coils are sealed by epoxy resin. Another transformer  $T_2$  based on the above methods is shown in Figure 8(b). The measured primary leakage inductance  $L_m=4.7\mu H$ . The leakage is greatly reduced.

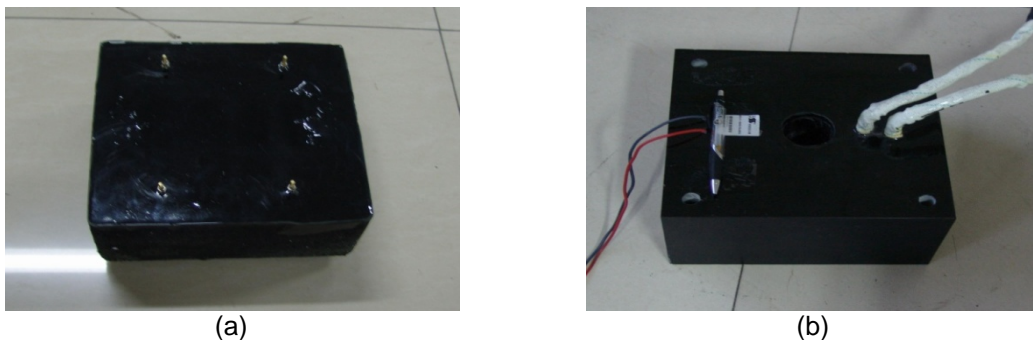


Figure 8. Two Transformers with Different Winding Dispositions (a) The high-frequency transformer  $T_1$  ;(b) The high-frequency transformer  $T_2$

### 5. The Experimental Results

Controller TMS320F240DSP chip is used for control circuit. In order to inhibit the larger current impact at the moment of closing the switch, the soft start with series resistance is used in main circuit. The input voltage is  $380 \times (1 \pm 0.1)V$ . The rectified DC voltage is about 540V. The withstand voltage of IGBT SKM200GB123D is 1200V. The turn-off current is 200A.  $C_r$  is 0.55  $\mu F$ .  $L_r$  is 125  $\mu H$ . The switching cycle of IGBT  $T_s$  is 105  $\mu S$ . The conduction time of the switch tube is 28  $\mu S$ . The charging current is constant in the charging process. The capacitor (600  $\mu F$ ) can be charged to 10 kV within 12s by charging power supply. The resonant peak current is 40 A. The average charging current and maximum output power  $P_{max}$  are:

$$I = C\Delta U / \Delta t = 0.5A \quad (11)$$

$$P_{max} = UI = 5000W \quad (12)$$

When the switching frequency  $f_s$  is 10 kHz, the charging requirements can basically met. The resonant current envelope and capacitor voltage of the transformer  $T_1$  are shown in Figure 9.

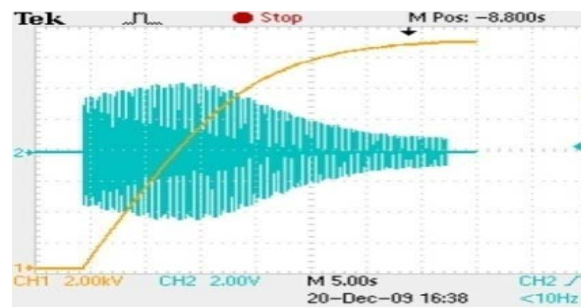


Figure 9. The Resonant Current Envelope and Capacitor Voltage

When the switching cycle  $T_s$  is 105  $\mu S$ , the driving voltage of IGBT is shown in Figure 10. The resonant current at peak became larger. The current flowing through the continued flow diode at peak became smaller. The switching device was working in the state of full soft switch in the process of charging. When the capacitor voltages are less than 0.5 kV, 5 kV and 10 kV, the resonant current waveforms are shown in Figure 11, Figure 12 and Figure 13.



Figure 10. IGBT Driving Voltage

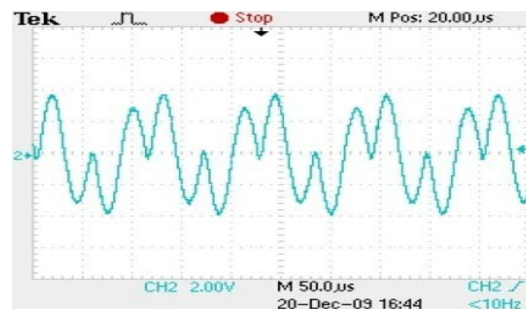


Figure 11. The Current (<0.5kV)

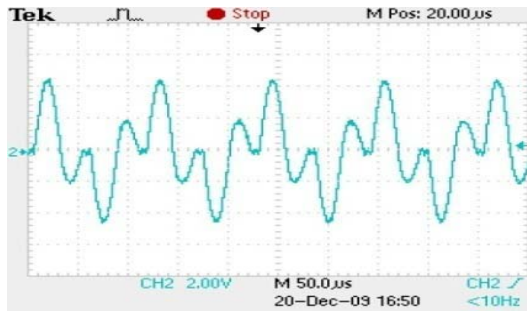


Figure 12. The Current (<math><5kV</math>)

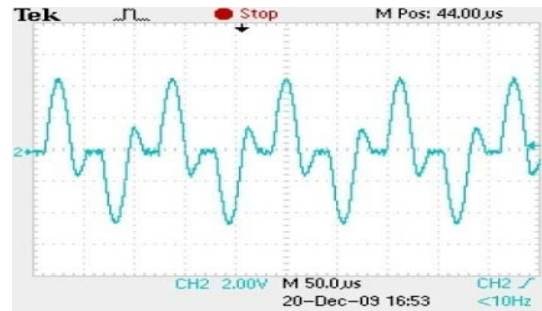


Figure 13. The Current (<math><10kV</math>)

The capacitor is  $600 \mu F$ .  $L_r$  is  $68 \mu H$ .  $C_r$  is  $0.77$ . The resonant period  $T_r$  is  $46 \mu s$ . The switching cycle  $T_s$  is  $95 \mu s$ . The turn-on time is  $25 \mu s$ . The bus voltage  $U_{in}$  is  $500 V$ . The high voltage capacitor is charged to  $14.8 kV$ . The waveforms of the capacitor charging voltage and the resonant current in the whole charging process are shown in Figure 14. The capacitor voltage  $U$  is  $10 kV$  at  $7.5 s$ . the peak resonant current is  $72 A$ . The constant current charging is realized. The average charging current and the maximum output power are:

$$I = C\Delta U / \Delta t = 0.8A \tag{13}$$

$$P_{max} = UI = 8000W \tag{14}$$

When the capacitor voltages are  $0.5 kV$ ,  $5 kV$  and  $10 kV$ , the resonant current waveforms are shown in Figure 15, Figure 16 and Figure 17.

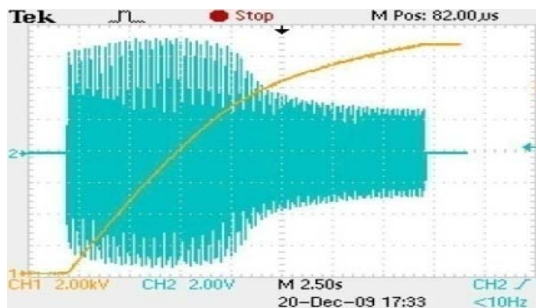


Figure 14. Current Envelope and Capacitor

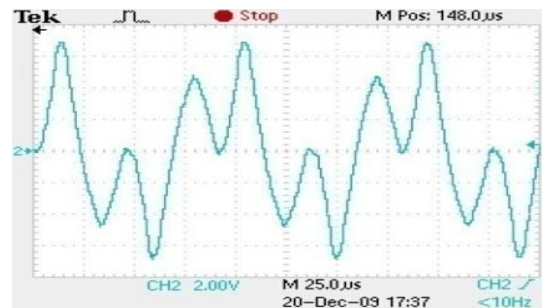


Figure 15. The Current at  $0.5kV$

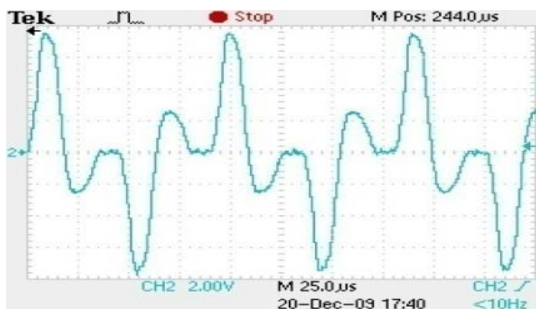


Figure 16. The Current at  $5kV$

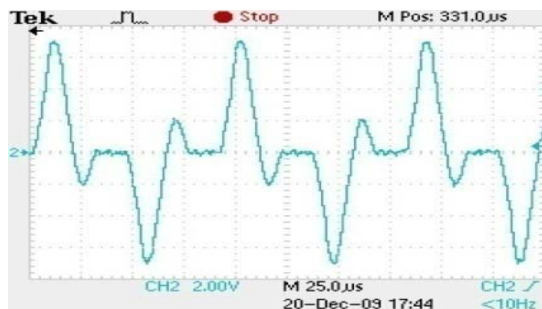


Figure 17. The Current at  $10kV$

Because of the influence of the distributed capacitor, the charging current is decreased when the capacitor voltage increasing. After a certain time, the resonant time of the continued flow in the diode is shorter. But, the resonant time of the conduction part in the switch tube is invariant.

## 6. Conclusion

The new charging control strategy and topology of the power supply for high voltage capacitor charging are designed. The performances of resonant soft switch are analyzed. Two new transformers with different winding skeleton structure are tested. Because primary and secondary coils are highly coupled in the new transformer skeleton structure, the leakage inductance is smaller. Because the parasitic capacitance in the transformer secondary is larger, the resonance cycle of the continued flow part in the resonant current diode is decreased before the capacitor voltage up to a fixed voltage value. To realize the constant current charging and improve the maximum output efficiency of the transformer, a series of technologies is adopted. The charging requirements can be basically met by above design. The constant current charging in the high voltage capacitor is realized. The new high frequency transformer has been applied to charging power supply for the electromagnetic emission.

## Acknowledgement

The authors wish to thank the engineers of the Key Lab of Industrial Computer Control Engineering of Hebei Province. This work was supported by a grant from the National High Technology Research and Development Program (863) for Military in 2009, China.

## References

- [1] Gao YH, Sun YH, Yan P. 20kJ/s High Frequency High Voltage Charging Power Supply. *High Voltage Technology*. 2008; 34(6): 1292-1294.
- [2] Wang L, Xu CM, Du HQ, Meng L H. State Estimation for Electrolytic Capacitor with Parameter Fitting. *TELKOMNIKA*. 2013; 11(8): 4461-4469.
- [3] Jian PZ, Yan X, Qiang H, Bisheng Z. The NC Power Supply Design of Large Current and Wide Frequency Pulse in SEAM. *TELKOMNIKA Indonesian Journal of Electrical Engineering*. 2013; 11(7): 3665-3672.
- [4] Wu Z, Qi D, Wei YM, Yuan G, Hua fu Z. Research on High Frequency Amplitude Attenuation of Electric Fast Transient Generator. *TELKOMNIKA Indonesian Journal of Electrical Engineering*. 2013; 11(1): 97-102.
- [5] Kumar Malliseti Rajesh, Lenine Duraisamy, Babu Ch Sai. A variable switching frequency with boost power factor correction converter. *TELKOMNIKA Indonesian Journal of Electrical Engineering*. 2011; 9(1): 47-54.
- [6] Zhong HQ, Xu ZI, Zou YP. Effects of Parasitic Capacitance on the Characteristics of Series Resonant Capacitor Charging Power Supply. *Chinese Journal of Mechanical Engineering*. 2005; 25(10): 50-57.
- [7] Zheng G, Jin S, Shi M. The Analysis and Processing of Distributed Capacitance in High-frequency High-voltage Transformer. *Electric and Electronic Technology*. 2002; 36(10): 54-57.
- [8] Dong JQ, Chen W. Modeling and Analysis of Capacitance Effect in High Frequency Switching Power Supply Transformer. *Chinese Journal of Mechanical Engineering*. 2007; 27(31): 121-126.
- [9] Zhao ZY, Gong CY, Qin HH. Affecting Factor Analysis of Distributing Capacitive in High Frequency Transformer. *Chinese Journal of Mechanical Engineering*. 2008; 28(9): 55-60.
- [10] Zhao CF, Yu Z, Wang ZY. The Design of High frequency Pulse Transformer. *Transformer*. 2003; 40(10): 6-8.
- [11] Zhong HQ, Xu ZX, Zou XD, et al. Research on High Voltage Soft Switching Power Supply. *High Voltage Engineering*. 2003; 29(8): 7-9